HighTech and Innovation Journal

ISSN: 2723-9535

Available online at www.HighTechJournal.org

HighTech and Innovation Journal

Vol. 5, No. 4, December, 2024

A Smart IoT Urban Flood Monitoring System Using a High-Performance Pressure Sensor with LoRaWAN

Matthew Christian L. Te [1], Joaquin Antonio T. Bautista [1], Shaquille Michael Edward V. Dimacali [1], Angelo Victor M. Lood [1], Marina Graciella M. Pangan [1], Alvin Y. Chua [1*]

[1] *Department of Mechanical Engineering, De La Salle University, 2401 Taft Avenue, Manila 0922, Philippines.*

Received 05 September 2024; Revised 14 November 2024; Accepted 22 November 2024; Published 01 December 2024

Abstract

The Philippines faces frequent flooding and significant loss of life and property. Current flood monitoring systems (FMS) are outdated, causing delays in information distribution and mitigation efforts. Therefore, this study presents the development of a pressure sensor-based system with LoRaWAN capability for continuous, remote flood detection. The FMS PVC housing design was iterated upon by changing lengths, diameters, and mounting systems. Moreover, each of the parts was modeled, simulated, and tested in ANSYS and evaluated with simulated real-world physical and environmental conditions. The FMS is equipped with LoRaWAN transmission and solar charging, which transmits data to The Things Network, where it is then visualized in Packetview. The resulting FMS design and mounting were robust and were able to withstand flooding conditions. The battery and solar panel are also sufficient in continuously powering the FMS. Moreover, the FMS was also able to withstand various tests with minimal sensor errors. The FMS holds the potential to enhance flood monitoring in the Philippines, offering localized, cost-effective, and near-real-time solutions for better disaster preparedness and response strategies. The FMS utilized the accurate theory equation that resulted in a flood height error as low as 1.12% in testing and 1.81% in rain. Furthermore, it is resistant to external disturbances as the system takes 0.5 seconds to stabilize, while continuous disturbances resulted in errors ranging from 0% to 3%.

Keywords: Flood Monitoring System (FMS); Pressure Sensor; LoRaWAN; Internet of Things (IoT); Solar Powered.

1. Introduction

Metro Manila experiences frequent and devastating floods due to its low-lying areas, heavy rainfall, and poor drainage systems. Since 1990, the country has averaged 20 typhoons each year within its area of responsibility [1]. These floods cause damage to infrastructure, disrupt the economy, and endanger public safety. Previous efforts to address this issue have led to the development of FMSs like the Nationwide Operational Assessment of Hazards (NOAH) program, with Hydrometeorological (HydroMet) Devices and Flood Information Network (FloodNET) among its component programs [2]. According to Lagmay et al. [3], the Metropolitan Manila Development Authority (MMDA) flood gauge reaches a maximum of 45 inches and is categorized as unpassable by vehicles and at human chest level.

Advancements in IoT applications have expanded the innovation of smart monitoring devices. Around the world, FMSs are equally as common and have taken many different forms. Classifications can be done through the type of sensor used, as well as the method of data transmission. Hassan et al. [4] made use of float switches, mechanical control

* Corresponding author: alvin.chua@dlsu.edu.ph

doi http://dx.doi.org/10.28991/HIJ-2024-05-04-04

elements that use buoyant levers to activate, and Global System for Mobile Communications-Short Message Service (GSM-SMS) transmission modems to create a successfully working device when used within a water tank. Rani et al. [5] used float switches but instead integrated the system with a Wi-Fi module. While float switches are a low-cost mechanical way to monitor water levels, they are limited in their accuracy because they only work when water crosses specific thresholds.

Ultrasonic sensors have also been found to be useful given their proximity sensing capabilities, as they provide a non-contact method to measure water level. Project NOAHs, Hydromet devices are an example that uses ultrasonic sensors with a GSM gateway to relay data sent to a sensor network [6]. Dswilan et al. [7] and Natividad & Mendez [8] executed the same concept with their FMSs. Zahir et al. [9] and Yuliandoko et al. [10] each created ultrasonic-based FMSs connected to Wi-Fi modules instead. The work of Yoeseph et al. [11] chose to take ultrasonic FMSs in another direction by using a newer, low-cost, and less power-consuming data transmission method in Long Range (LoRa) communication, which transmits data through radio waves. The study concluded that achieving a data delivery delay of 0 ms is possible using LoRa. Zakaria et al. [12] expanded this further by using the LoRa Wide Area Network (LoRaWAN), which pushes the range of the system even further. Although ultrasonic sensors are effective and mostly accurate, they can also suffer from increased error values when the sensor comes close to water surfaces, with distances less than 2 cm, causing more than 10% differences [13]. Koh & Mustafa [14] utilized LoRaWAN in their solar-powered FMS with an ultrasonic sensor and a buzzer. The results described the performance of its device and its ability to activate the buzzer once a specific threshold was reached. The study showed that using a LoRa module allows the sensor to send data to the receiver, showing the flexibility for the components to be housed separately. However, this was done in a controlled environment where water was measured from a basin and was not tested for outdoor conditions.

Image processing, which analyzes camera-taken pictures, has also been used in FMSs. Tolentino et al. [15] and Lo et al. [16] process the sent photographs through different filters that allow flood heights to be measured. Moreover, Hashemi-Beni et al. [17] used deep-learning segment gauges from images using Mask-RCNN in real-time flood monitoring even though the images are distorted from camera movement or there is a little light source at nighttime. This method has the potential downside of being power-intensive due to the need for a camera and the uploading and processing of pictures.

There are even systems that make use of multiple sensors at a time. Bande & Shete [18] utilized an ultrasonic sensor, rain sensor, and humidity sensor in their FMS to collect flooding data. It was then used to create flood prediction models. Sadhya et al. (2024) [19] utilized both LoRa and GSM-SMS for their FMS device, which had an ultrasonic and water flow sensor and a buzzer. It produced similar results to [14], where the device successfully measured the water level and activated the buzzer at the given threshold. Saparudin et al. [20] performed a case study on a real-time FMS device using a mobile LoRaWAN IoT gateway. Conducted at the Muar River in Malaysia, the devices consisted of an ultrasonic and a raindrop sensor module housed in PVC tubes powered by a solar power source; its gateway was housed in a UAV for enhanced deployment. Data measurements focused on determining the behavior of high and low tides experienced by the river; their results suggest that the delays in high tide measurements across each device were caused by their distances. The study highlighted the potential of creating a prediction model and the importance of the distance capabilities of each device concerning the gateway. Predictive forecasting continues to be a theme for FMSs with multiple sensors, as Gunanandhini et al. [21] employed an ultrasonic sensor, a water flow sensor, and an anemometer in a solar-powered real-time FMS. The system used LoRaWAN and Message Queuing Telemetry Transport (MQTT) for data transmission but was also capable of sending alerts to emergency responders using GSM-SMS.

Each flood monitoring sensor type comes with its strengths and weaknesses. Pressure sensors circumvent many of the issues found while using other sensors. Float switches have mechanical parts that are easily worn and have discrete measuring intervals, unlike pressure sensors that do not have any moving parts and can provide continuous data. Other sensors can also provide continual output but come with their drawbacks. Image processing can be energy intensive, while ultrasonic sensors can be susceptible to errors when debris or foam is present. The bulky fence housing required for ultrasonic FMSs makes installation take up a larger area and comes at a higher cost. Pressure sensor-based systems tend to not have these disadvantages but require proper sealing. For example, the proposed FMS in this article only requires a narrow tube where water can enter.

Pressure-based FMSs have a history of usage. Garcia et al. [22] used a ground-based pressure sensor and rain gauge to measure flood height and for flood prediction models. The ground-based configuration requires the electronics to be closer to the ground, requiring a mesh cage to prevent tampering. By adopting an open-ended manometer setup, the pressure sensor location is much higher, and the electronics can be placed out of reach. Azid et al. [23] present a pressure-based FMS that acts as an open-tube manometer. Pressure increases uniformly as the water levels rise around and into a tube with a singular open end. The system transmits their data through GSM-SMS, resulting in a reliable and cost-effective system. However, GSM-SMS is prone to long transmission delays and requires expensive and large infrastructures such as cell towers to function. Moreover, the FMS frame is made of metal, prone to rusting. By adopting LoRaWAN transmission, the long transmission delays are minimal and require large and expensive infrastructures to transmit data. Moreover, using PVC pipes instead of metal housing decreases the overall price and standardizes the materials while maintaining their structural integrity. Dublin et al. [24] used the same principles to make their FMSs but instead used Wi-Fi for the data transmission method. Success was found in the accuracy of the system, but problems surrounding the unreliability of the Wi-Fi connection were also highlighted. Similarly, the adoption of LoRaWAN can alleviate this problem.

The need to improve and expand these systems to ensure effective monitoring, early warning, and disaster response still remains. It could be gathered from the previous studies that the data transmission methods may still have the potential to improve through LoRa, which still has limited documentation when compared to the more popular data transmission methods. More testing for pressure sensors used within open-tube manometers could also be used to verify the accuracy and reliability of this method of flood monitoring.

This article describes a novel FMS device for urban areas that uses a high-performance pressure sensor with LoRaWAN capabilities. The theoretical basis behind calculating flood heights using the device will first be explained before the mechanical design process for the FMS's different components is shown. Simulations and tests will then be presented to show not only the viability of the FMS, but its accuracy, response time, and capability to perform in real-life scenarios. The combination of pressure sensors and LoRaWAN Transmission marks a significant advancement in urban flood monitoring by enabling near real-time, long-range data transmission with low power consumption, which is crucial for continuous and reliable operation in both densely populated areas and rural areas. The system's design leverages the strengths of LoRaWAN technology to provide scalable and cost-effective FMS, offering a robust solution to enhance local readiness and response against flooding events.

2. Theoretical Considerations

2.1. Pressure and Water Level

The basic principle of the flood-monitoring device used for this study was adapted based on the inverse barometric effect discussed by Dublin et al. [24]. Through measuring data through pressure sensors and processing it through formulas, the height of a flood can be ascertained.

The downward-facing tube of the device traps air as water height increases and blocks the opening. The water that covers the open end will continuously exert pressure onto the air inside, simultaneously increasing its pressure as well. This results in an internal pressure that is higher than the atmospheric pressure that can be recorded from outside the PVC pipe. The air inside the tube also applies pressure on the water inside the tube, making it rest at a noticeably lower height than the outside water level. Figure 1 is an illustration of the inverse barometer effect taking place as well as the theory and relationship between the pressure and water level.

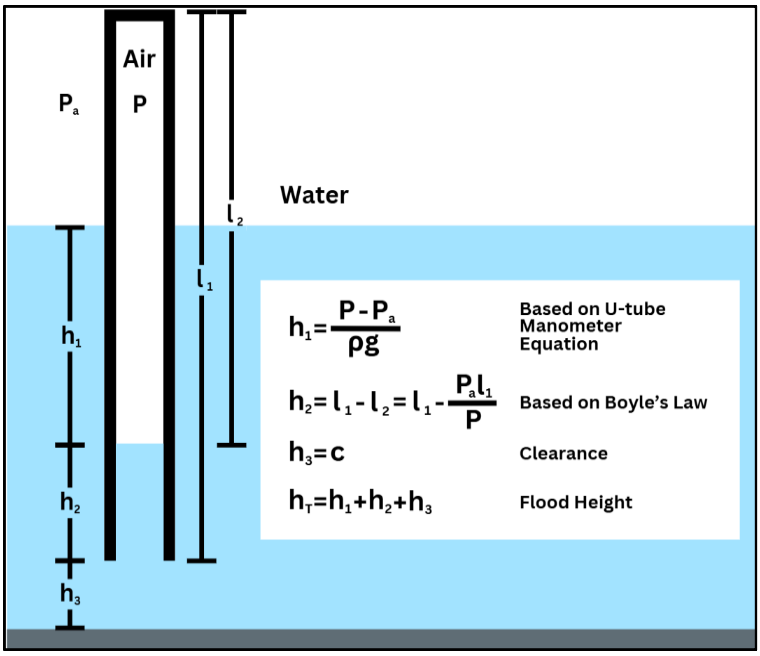

Figure 1. Flood Monitoring System Theoretical Concept

Equation 1 can be used to calculate total flood height:

$$h_T = h_1 + h_2 + h_3 \tag{1}$$

where h_T is total flood height, h_1 is the difference in height between the water inside the tube and the actual flood height, h_2 is the height of water inside the tube, and h_3 is the clearance, or the height of the gap between the floor and the opening of the tube. h_3 is a value that needs to be noted upon installation.

The setup can be likened to an open-ended U-tube manometer as one side is exposed to atmospheric pressure while the inside experiences a different pressure that causes water levels to differ. To calculate the difference in water level between the outside and inside of the tube during a flood, Equation 2, which is used for open-ended U-tube manometers, can be used:

$$h_1 = \frac{P - P_a}{\rho g} \tag{2}$$

where h_1 denotes the water level difference, P is the pressure inside the tube when flood waters are present which can be obtained using the pressure sensor within the tube, P_a is atmospheric pressure, ρ is water density which is assumed to be a constant 1000 kg/m^3, and g is acceleration due to gravity which is a constant 9.81 m/s^2.

Following Boyle's Law, Equations 3 to 6 are used to determine the height of water within the tube.

$$h_2 = l_1 - l_2 \tag{3}$$

$$l_2 = \frac{P_a l_1}{P} \tag{4}$$

$$V_1 = \frac{\pi}{4} d^2 l_1 \tag{5}$$

$$P_a V_1 = P V_2 \tag{6}$$

where l_2 is the height of water inside the tube starting from the opening, l_1 is the total height of the entire tube, h_2 is the height of air present within the tube, V_1 is the volume of air within the tube in atmospheric pressure, V_2 is the volume when the air within the tube is compressed by flood waters, and d is the diameter of the tube.

Through the substitution of Equation 4 into Equation 3, the water level inside the tube can be calculated:

$$h_2 = l_1 - \frac{P_a l_1}{P} \tag{7}$$

Substituting Equation 2 and 7 into Equation 1 nets the final flood height formula:

$$h_T = \frac{P - P_a}{\rho g} + l_1 - \frac{P_a l_1}{P} + h_3 \tag{8}$$

The inclusion of l_1 within the formula allows for adjustments to be made in cases where longer tubes are necessary.

3. Material and Methods

The methodological framework of the study is shown in Figure 2. It is divided into three parts, mechanical, electronics, and software. The mechanical portion focuses on the design, simulation, and fabrication of the FMS body, the electronic portion focuses on the electronic components of the FMS, and the software focuses on programming to enable LoRaWAN transmission. This all combines into the performance testing of the FMS.

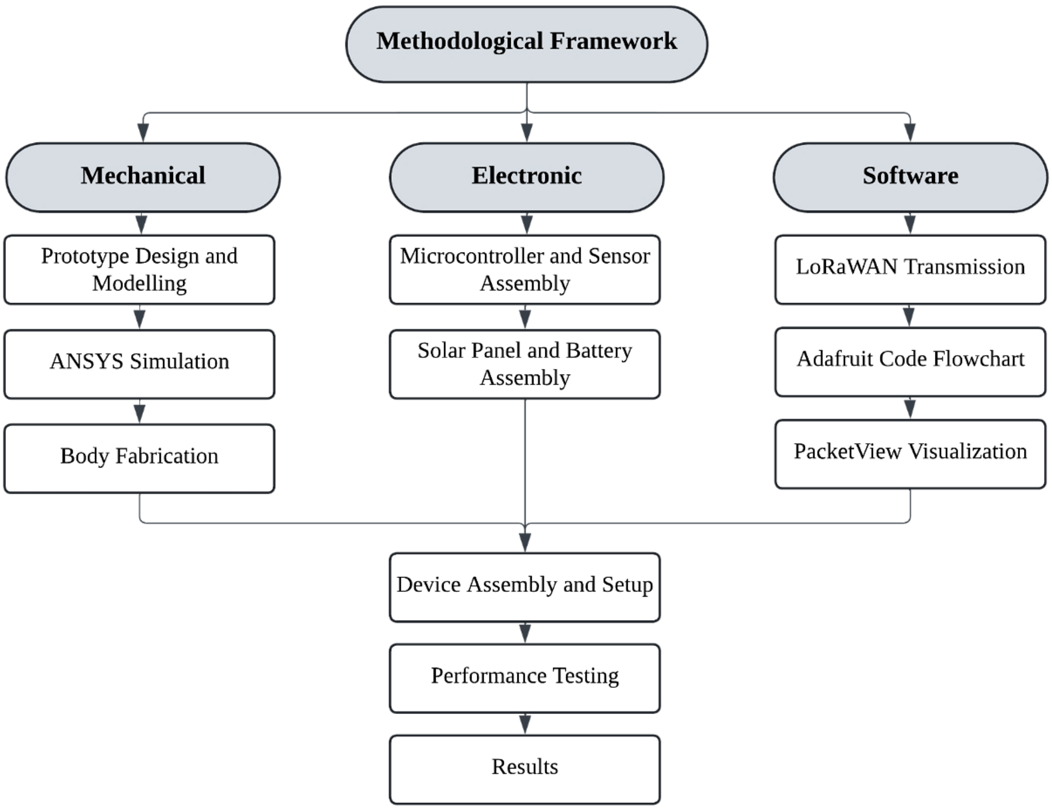

Figure 2. Methodological Framework

3.1. Mechanical: Prototype Design, Modelling, Simulation, and Fabrication

The main structure of the FMS consists of a main PVC housing and an electronic box as shown in Figure 3. The electrical wiring connects the PV housing to the electronic box. The FMS is securely installed in a post using a metal post mounting bracket strap since it is manufactured to withstand environmental elements while being able to bear the load. The bottom is in contact with the ground to read the flood height.

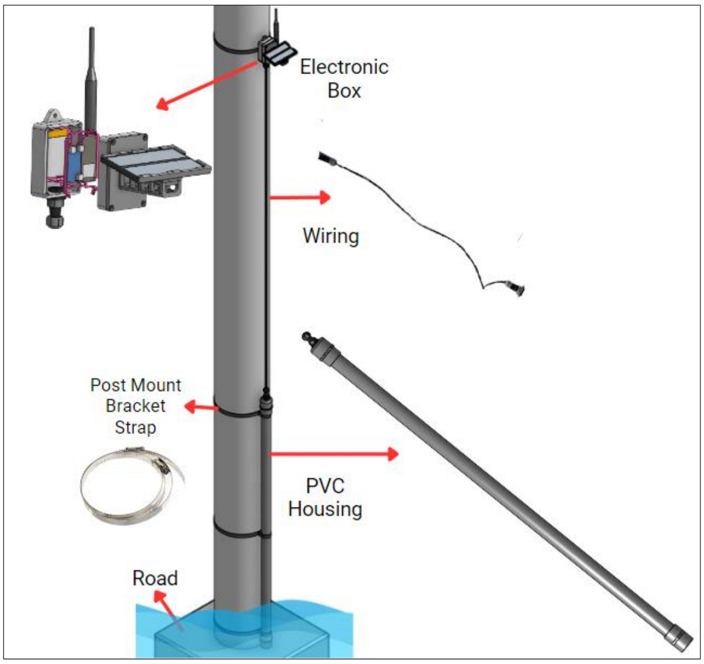

Figure 3. FMS Configuration

3.1.1. PVC Housing

As shown in Figure 4, the PVC housing properties include air-tight, water-resistant, and modularity to enclose the flood water. It consists of a 1.0-inch diameter and 1-meter PVC pipe, a male-threaded pipe adapter, a female-threaded pipe adapter, and a female-threaded end cap with an SP13 IP68 cable connector. The main housing is chosen to be 1.0 inches so that the pressure sensor can fit within its enclosed space. At the end cap, a custom-made pressure mount is fastened to act as a pouch, which holds a DPS310 pressure sensor at the top. This sensor reads the pressure within the enclosed space below. For modular extensions, 0.5-meter increments of PVC are also used. After that, the housing is painted gray for an inconspicuous design when attached to the post.

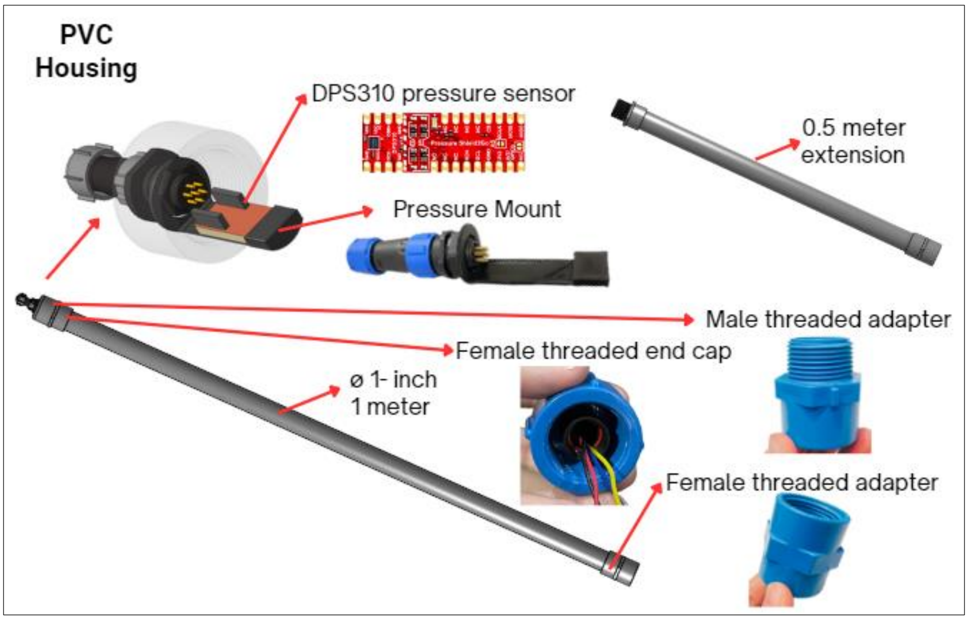

Figure 4. PVC housing

3.1.2. Electronic Box

As shown in Figure 5, the electronic box is an IP65 Twinbox Weatherproof Enclosure. Custom electronic compartments were designed and made to place the electronics within the system. Attached to it is a solar panel mount that mounts the solar panel which charges the battery. To extend the range of the LoRaWAN transmission, an antenna is connected and placed outside the box.

Figure 5. Electronic Box

3.2. Electronics: Microcontroller and Solar Assembly

The electronics inside of the electronic box consist of an Adafruit Feather M0 RFM95W, which translates and transmits the data collected from the pressure sensor to a local LoRaWAN gateway; a CN3065 Mini Solar Lithium Battery Charger Board Lipo Battery Charging Module, which stabilizes the charging and power delivery; 1000 mAh Lithium - Polymer rechargeable battery, which powers the system; a 1W 6V solar panel, which charges the battery; and a 900 MHz antenna, which transmits that data (see Figure 6).

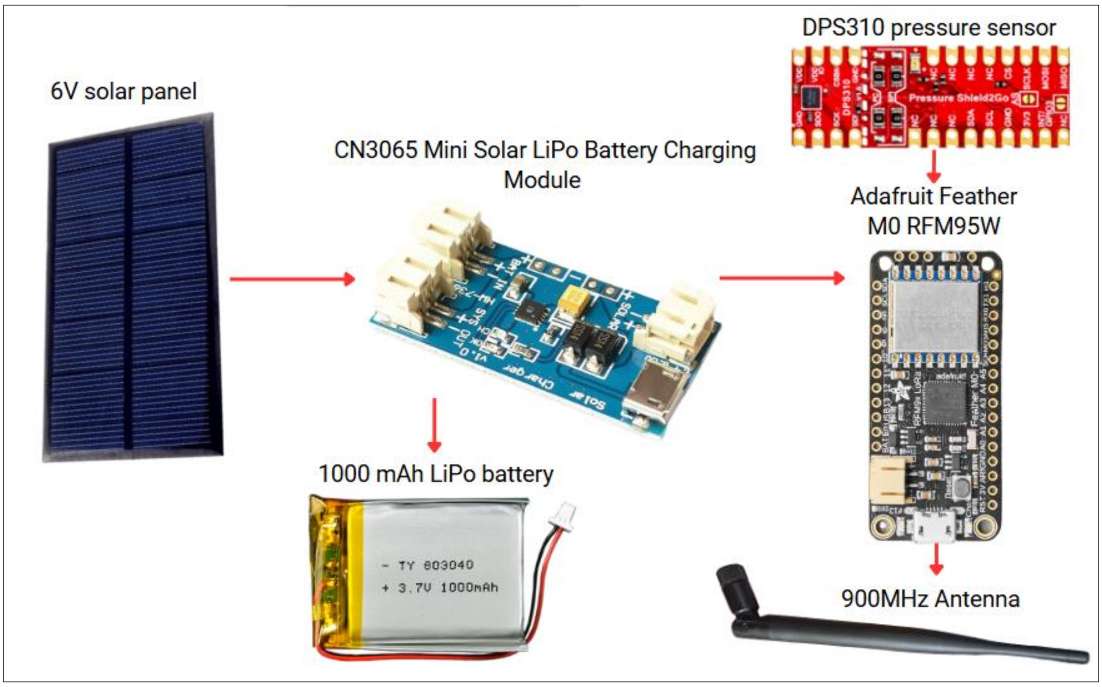

Figure 6. Electrical Configuration

As shown in Figure 7, the wire connectors connect the electric wiring between the pressure sensor within the PV housing and the microcontroller within the electronic box. Since it is crucial for them to be environment and water-resistant, modular IP68 SP13 connectors are used as it is rated to survive dust, water splash, and up to 1.5 meters freshwater submersion for 30 minutes. Moreover, the system utilized two connectors, one in the end cap of the housing and another in the electronic box.

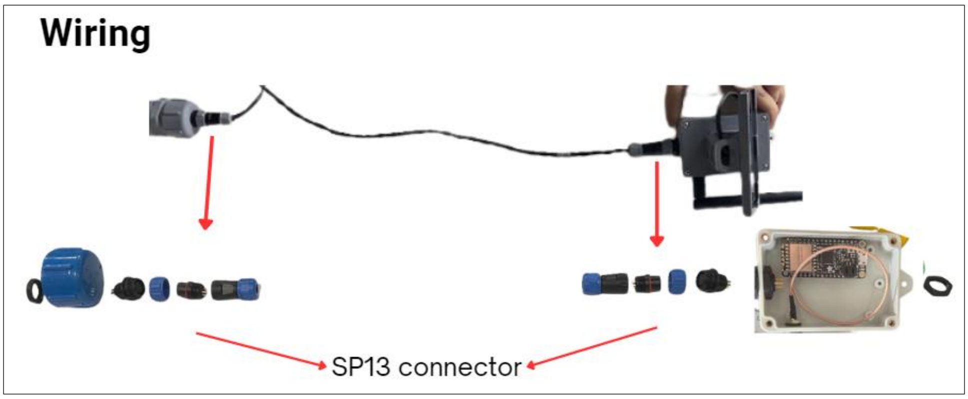

Figure 7. Wiring

3.3. Software: LoRaWAN Transmission and Visualization

LoRaWAN was integrated into the system as it transmits data at long ranges through radio waves at low power consumption. For data communication and visualization in a network server, the group consulted with a company that serves LoRaWAN communication locally, Packetworx. To integrate LoRaWAN, the pressure readings from the sensor are relayed to the Adafruit Feather M0 microcontroller which then transmits the data to a local LoRaWAN gateway using LoRa. The gateway then transmits the data to The Things Network server to process the data. The process data is then viewed through the Packetview visualization application as shown in Figure 8.

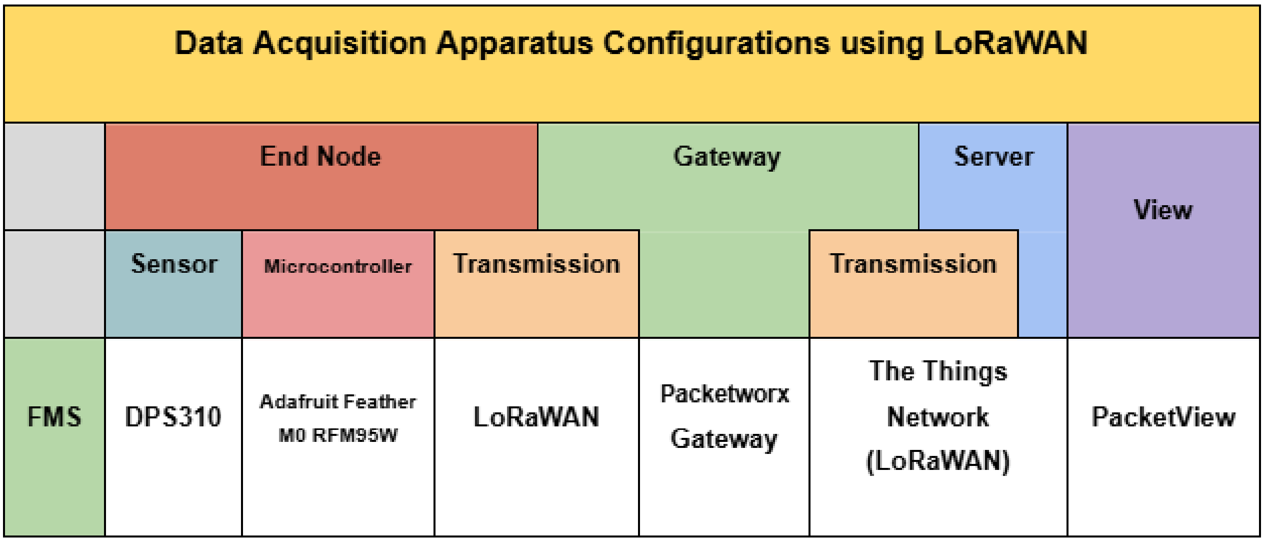

Figure 8. LoRaWAN Data Acquisition Configuration

For the LoRaWAN transmission to be operated, the Adafruit Feather M0 microcontroller, The Things Network server, and Packetview must be programmed to accommodate the system. Figure 9 displays the Arduino code flowchart used in programming the Adafruit Feather M0, which was adapted from the Arduino LoRaWAN LMIC Library. It begins with the initialization of the libraries used in the program, the LoRaWAN and sensor, the variables used, and the security keys to connect the FMS to the server. Once initialized, the transmission can begin, and a join request can be transmitted. If there is a nearby gateway, it will assess the join request and reply with a join accept if the join request is valid. If not, the gateway will not reply, and the code will time out with no join accepted. When the join request is accepted, the DPS310 sensor will begin measuring the pressure and temperature. Once measured, the data will be encoded into four-byte payloads for the LoRaWAN transmission. Next, it will transmit the data. Once the transmission is complete, the code will hibernate until the next transmission window, where it will measure the next set of pressure and temperature data to be transmitted.

A LoRaWAN gateway was installed on the rooftop of the St. Joseph (SJ) building in De La Salle University (DLSU) and was used to send data to the servers. The gateway's operating frequency was specified at 868 MHz. Data was being sent to the online server, The Things Network; and data visualization was done using Packetview, a dedicated online data visualization platform provided by Packetworx. The data sent to the server was decoded and formatted from the byte payloads to a common coding language like JavaScript. From then on, the data in recognizable data are customized to a more user-friendly visualization using ThingsBoard Expression Language (TBEL) or JavaScript. The Packetview shows the processed data of pressure, temperature, and flood heights using graphs which were accessible to end users as shown in Figure 10.

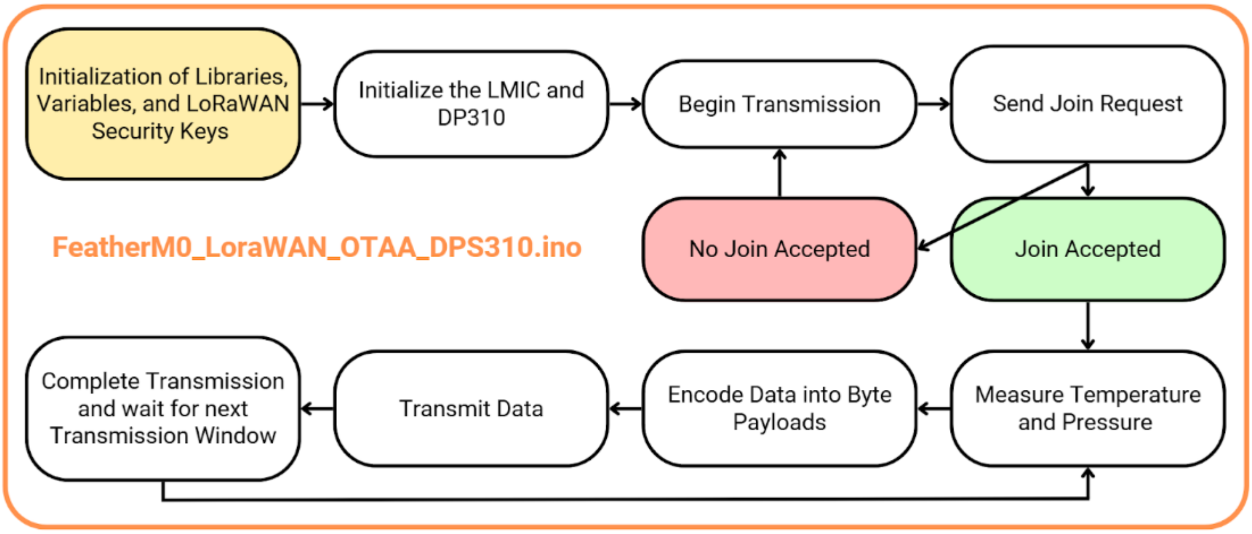

Figure 9. Software Flowchart of the Adafruit Feather M0 Arduino Code

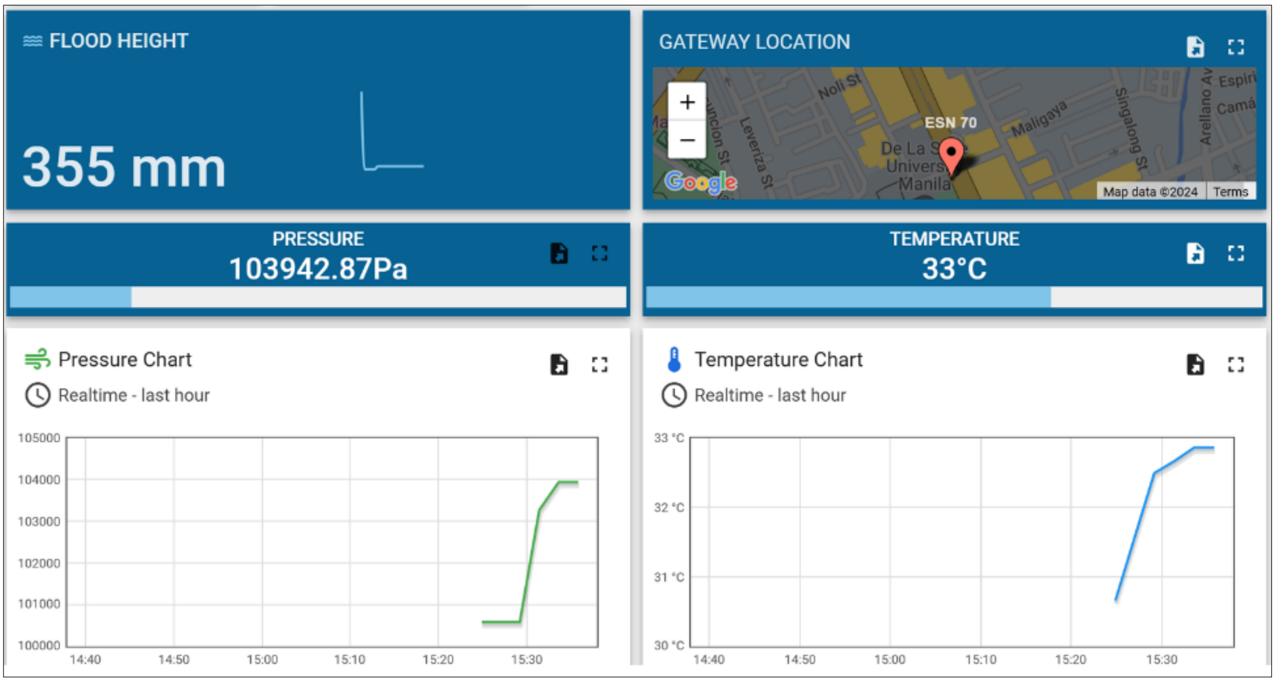

Figure 10. Packetview visualization

3.4. Performance Testing

3.4.1. Calibration and Theory Equation Testing

To ensure the accuracy of the FMS, calibration was performed using a clear acrylic tube and tape measure. Pressure readings were taken at various water heights and plotted to produce a calibration equation. This was also compared to the theory equation shown in Equation 8. The theory equation, based on the inverse barometric effect, is used to account for variables such as atmospheric pressure and water density. This equation provides a more flexible and accurate measurement compared to the calibration equation. Also, the system was tested with a PVC elbow fitting to accommodate installation constraints that may occur in certain areas. The test was conducted using a 1-inch PVC pipe with 90-degree elbow bends. The flood water height for the elbow was also calculated based on the approximation shown in Figure 11 using Equation 8. Moreover, liquids with different densities, which are Pasig River water, palm oil, and tap water are used to test the reliability of the equation.

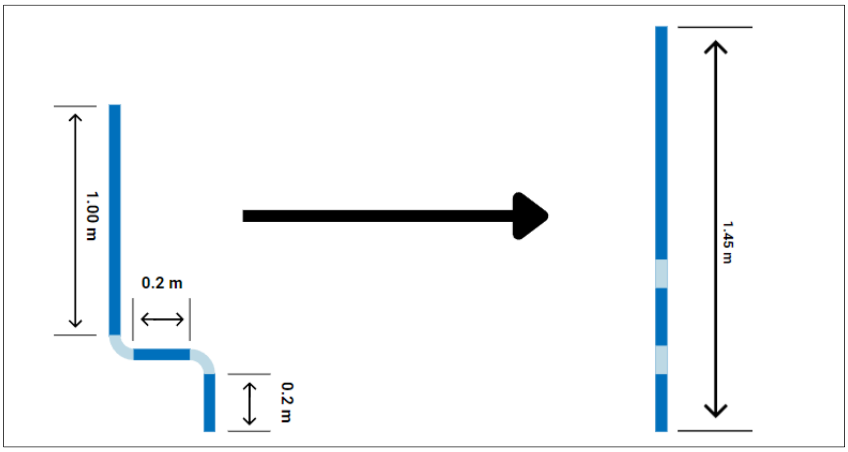

Figure 11. Elbow Test Tube Height Approximation Diagram

To further test the theory equation, iterations on the tube diameter and length of the main PVC housing were tested. Since the PVC housing needs to fit the pressure sensor (14.0 mm × 38.5 mm × 2.5 mm) within its enclosed space, varying diameters iterations of 0.75 in, 1 in, and 1.25 in commercial standardized PVC pipes were used in testing. The base housing is chosen to be at least a 1-meter height following MMDA's gauge [3]. The 45 in height is rounded down to 1 m for simplicity based on standard PVC tube lengths. However, flood height can exceed 1 m. To accommodate this, modular tubes can be added to the 1 m base length at 0.5 m intervals. From this, varying heights of 1-meter, 1.5-meter, and 2-meter heights were tested.

3.4.2. Flood Surge & Disturbance Testing

Experiments were conducted to test how quickly the FMS could adapt to sudden flood surges. The methodology involved setting up the FMS at various height clearances above ground level, starting at 0 cm up to 3 cm with 0.5 cm increments in between. In a controlled environment, a flood surge was simulated by suddenly releasing a set volume of water, consistent throughout all trials. Moreover, various flow disturbances were simulated to test the system's response. The tests involved introducing disturbances to a set volume of water in a big container using four methods: paddling, shaking, shaking for 5 seconds, and one large continuous shake. The recorded data was then brought into MATLAB for graphical analysis.

3.4.3. Power & LoRaWAN

When using LoRaWAN, the system transmits pressure readings to a local gateway, which sends the data to the IoT network server for processing and visualization. The Adafruit Feather M0, The Things Network server, and Packetview are programmed to accommodate the system. The FMS's power consumption was also validated by observing the longevity of the system when powered by a small battery and solar panel.

3.4.4. Endurance, Rain Simulation, and Actual Rain Test

An endurance test was performed to ensure the sensor's stability over long periods. The pressure sensor was configured to gauge a water height of 100 millimeters at intervals of 5 seconds over a duration of 72 hours. This data was then compared to another pressure sensor measuring atmospheric pressure every 5 minutes to compare their trends. Next, the overall function of the FMS was tested with a simulated rain shower, mimicking actual installation conditions. For the testing, the shower ran continuously while the researchers observed the rise in water level inside the container. Actual water height over time was compared to the recorded water height over time for three trials. Finally, the system was also set up outdoors to test its functionality in actual rain conditions. The testing procedure for this setup is the same as the rain simulation tests.

3.5. Overall System

As shown in Figure 12, the pressure data collected by the FMS was relayed to the electronic box via wires. This was then transmitted to the Packetworx LoRaWAN gateway using 868 MHz LoRaWAN frequency. From this, the gateway then transmits the data to The Things Network LoRaWAN server over the internet, where it will be processed. The processed data is then viewable by the end user through the Packetview web visualization application.

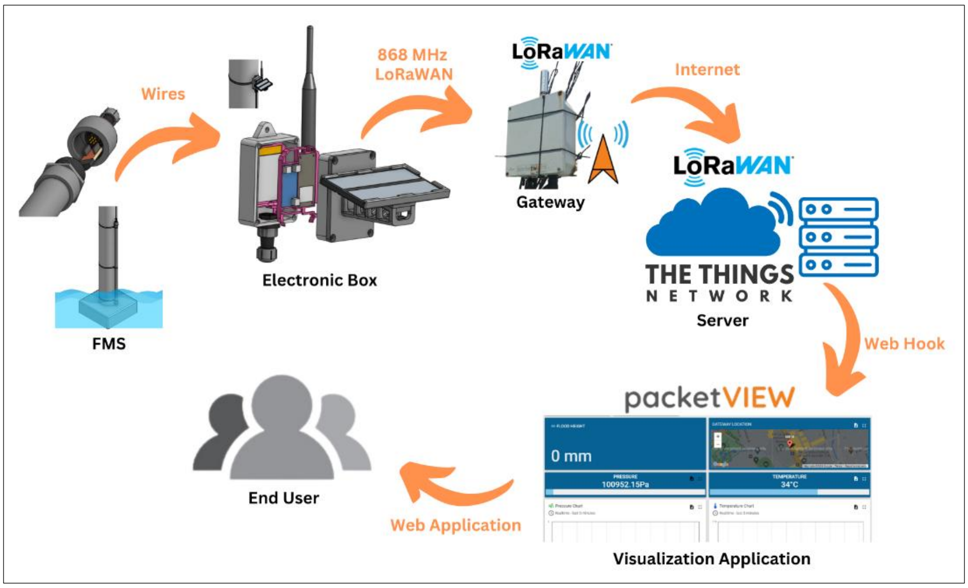

Figure 12. Flood Monitoring System Overall Design

4. Results and Discussion

4.1. ANSYS Simulation

The analysis of the device was focused on its physical capability. Existing literature focused on the performance of the data hardware. Compared to Arce et al. [25], the simulation was only limited to the design of the PVC end cap which houses the wire connector. This simulation through ANSYS expanded on the determination of the durability of the entire device fastened to a solid post, representing its operation during harsh weather. The PVC mount finite element analysis is as shown in Figure 13. The deformation was computed having the maximum recorded value of 0.216 mm, which was experienced at the bottom half of the pipe. With the rated ultimate stress of PVC, the computed factor of safety was also shown, which produces a high factor of safety. This suggested that the amount of force to destroy the PVC pipe could only be produced by heavier loads such as a vehicle directly hitting it, not by the forces applied by flood water. Therefore, through proper fastening, the device will be durable for operation. However, it is to be noted that this only represented an applied static force. Thus, further validation of the results using variable load conditions is required.

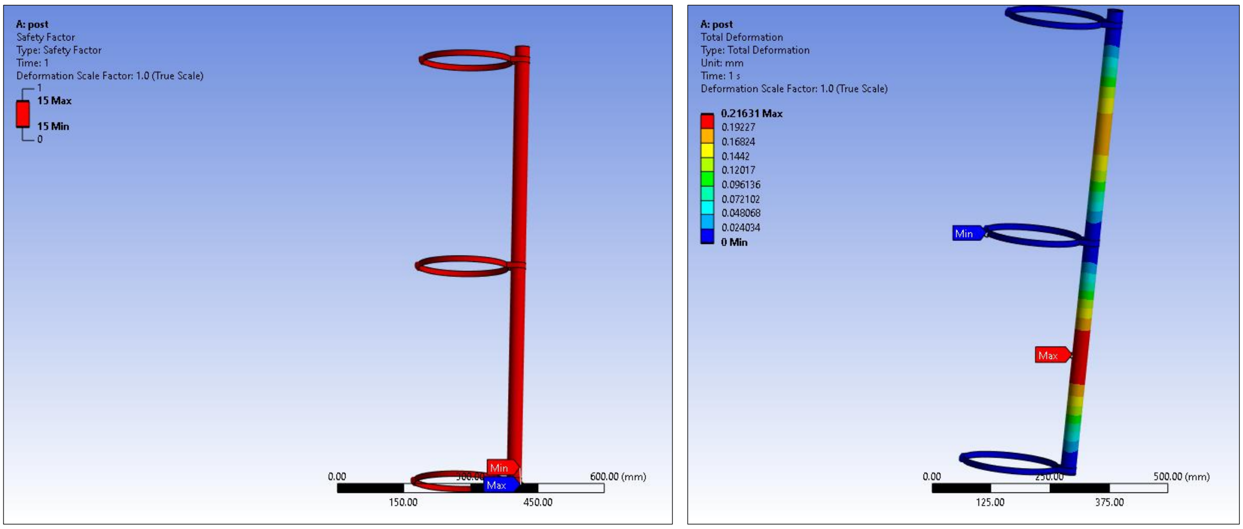

Figure 13. PVC Mount Finite Element Analysis

4.2. Performance Testing

Many different tests were conducted to test the performance of the FMS. Firstly, the FMS was calibrated and tested, resulting in an average percent error of 1.64% and standard deviation of 4.48 mm. The low percentage error of the calibration equation shows that the system was properly calibrated to measure the flood height. However, it is limited only to a certain atmospheric pressure and becomes inaccurate as time passes. To make the system operable regardless of atmospheric pressure, the theory equation was used as shown in equation 8. This resulted in an average error of 2.16% and standard deviation of 3.82 mm. The error and standard deviation comparison between the calibration and theory equation can be seen in Figure 14. The theory equation also exhibited low percentage errors comparable to the calibration equation, demonstrating its accuracy. Moreover, this also demonstrates the accuracy of the pressure sensor, which can measure pressure accurately up to ±0.06hPa. The error can be mostly attributed to human error, small changes in atmospheric pressure, and disparities in the actual internal sensor height. When compared to Arce et al.'s results, the percentage error calculated was lower but had a similar trend. This shows that the system was able to recreate and improve upon Arce et al.'s results. Furthermore, the accuracy for the proposed system is higher than in FMS of various literatures such as by Lee et al. [26] with 90% accuracy, William et al. [27] at 92%, and Prakash et al. [28] at an average of 97%. These literatures used different FMS methods in their studies, which also highlights the high accuracy of using a pressure-based FMS.

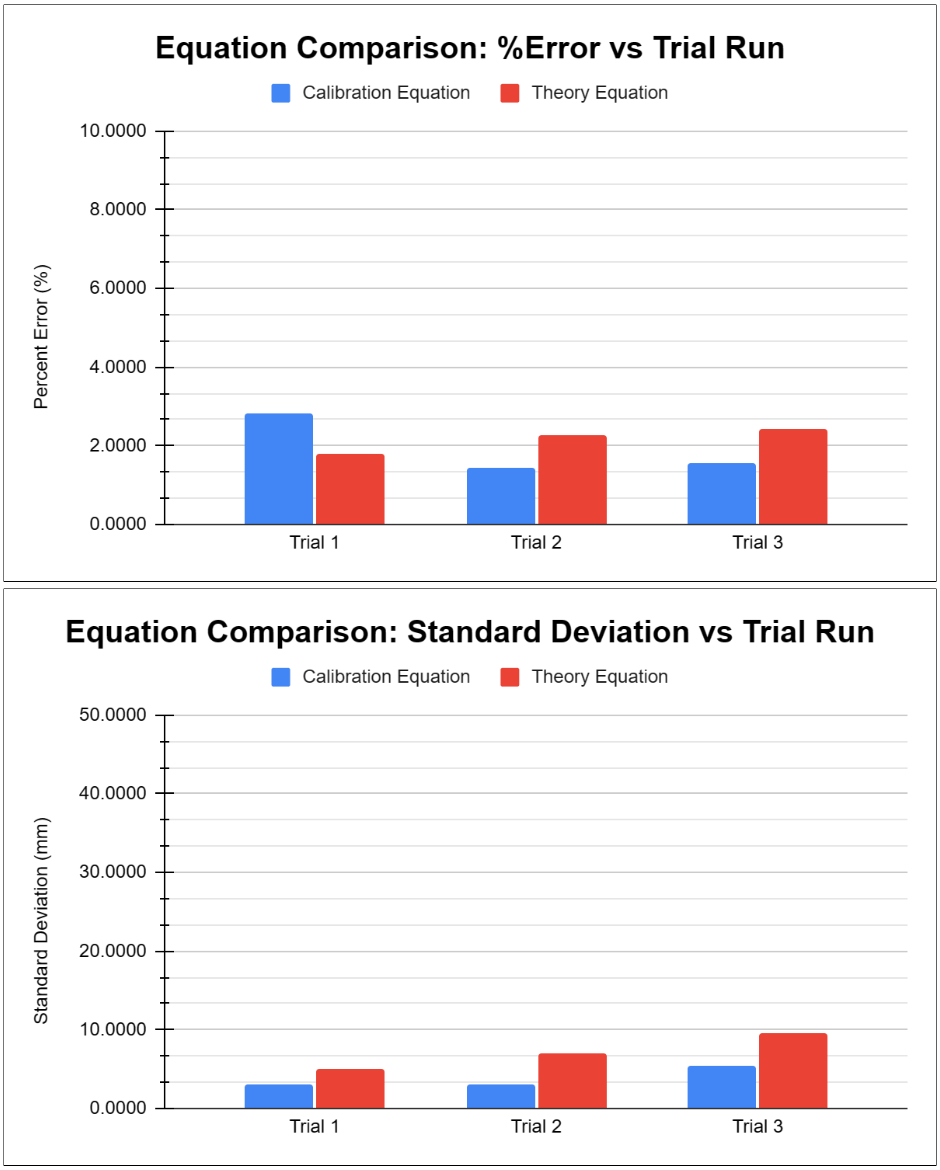

Figure 14. Percentage Error and Standard Deviation comparison between the Calibration Equation and Theory Equation

When varying the tube length, tube diameter, and fluid density of the theory equation, the following results were produced: For the tube lengths, the 1 meter tube length showed a percent error of 2.16% and standard deviation of 7.15 mm, the 1.5 meter tube length showed a percent error of 2.44% and standard deviation of 8.34 mm, and the 2 m setup had a percent error of 1.66% and standard deviation of 5.54 mm. As for the tube diameters, the 0.75-inch diameter had a percent error of 0.88% and standard deviation of 1.95 mm, the 1-inch diameter had a percent error of 2.16% and standard deviation of 7.15 mm, and the 1.5-inch diameter had a percent error of 2.35% and standard deviation of 6.61 mm. Finally, for the fluid densities, the tap water with density of 1000 kg/m^3 had a percent error of 2.16% and standard deviation of 7.15 mm, the flood water with density of 1000 kg/m^3 had a percent error of 1.12% and standard deviation of 3.92 mm, and the palm oil with density of 905 kg/m^3 had a percent error of 1.75% and standard deviation of 3.94 mm. All the variations in length, diameter, and density resulted in low percentage errors, displaying the accuracy and reliability of the theory equation. This also demonstrated that the theory equation can be applied to varying designs of the flood monitoring system, so long as the core principle remains.

When testing the elbow arrangements, the system using the 90-degree elbow with the standard theory equation setup with an indicated height of 1m showed a percent error of 6.14% and standard deviation of 13.67 mm. When using the approximation of a height of 1.45m, the percent errors and standard deviations across three trials were reduced by at least 3.62% and 8.86 mm respectively. This showed that the approximation was able to reduce the error in measuring flood heights and produce an acceptable percentage error with minimal adjustments to the system.

Moreover, to test the robustness of the FMS under flood surge and flow disturbance were performed. The results showed that the FMS was resistant to disturbances as it can stabilize within 0.5s when tested up to 30mm as shown in Figure 15. For flood disturbance, it was found that as the flood disturbance increased in intensity, so did the measured flood water height deviation as shown in Figure 16. However, when the error was calculated, it was found to be mostly within 0 to 3%, which was acceptable. This was a result of the thin and circular design of the flood monitoring system, which reduces the amount of force it absorbs and keeps it better fastened to the post. Furthermore, because the flood height measured is based on the flood water height inside the tube, the containment makes it less susceptible to disturbances and keeps the readings steadier. Therefore, it can be said that the FMS is able to withstand flood disturbances and vibrations.

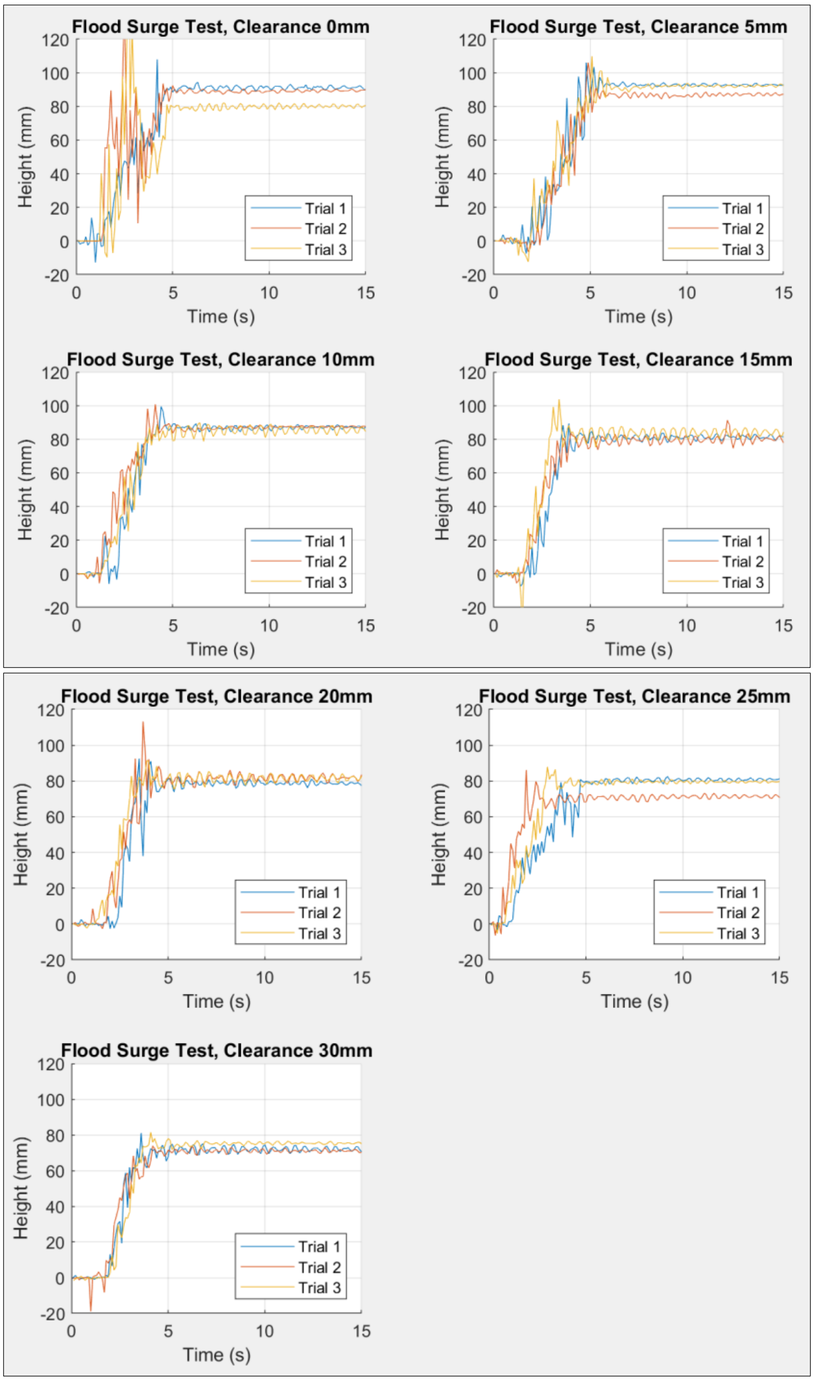

Figure 15. Flood Surge Test Data

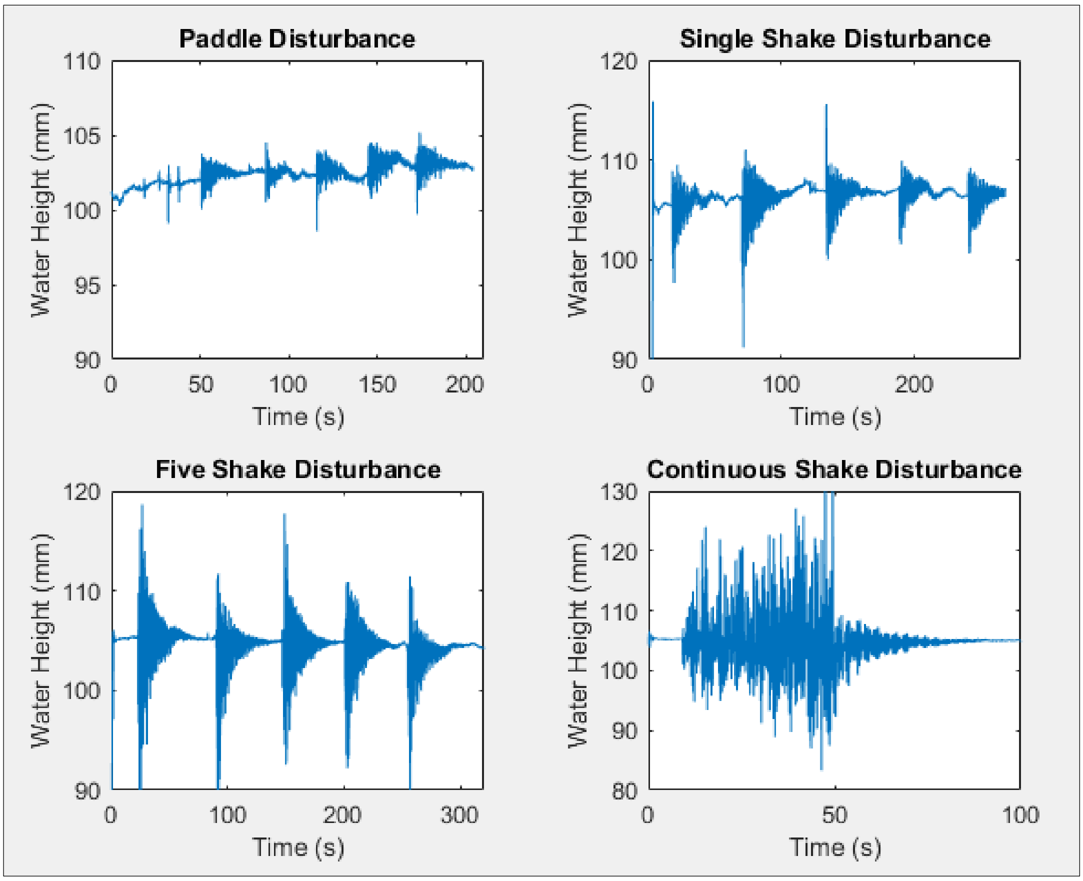

Figure 16. Flood Disturbance Test Data

As for the variation of atmospheric pressure, it was found that a singular atmospheric pressure within a range of 1-2 hours can be used in the theory equation with minimal increase in errors. Furthermore, the atmospheric pressure can be gathered from a centralized city source. Therefore, an average historical atmospheric pressure constant table was proposed for every hour, for every month, from May 2023 to May 2024 as shown in Table 1. When the dataset was tested in comparison with actual measured atmospheric pressure, the average percentage error was 0.167%. This finding is significant as it removes the requirement for an additional atmospheric pressure sensor in the FMS, decreasing the overall cost of the system with minimal impact on its accuracy.

Table 1. Philippine Atmospheric Pressure Constant Table According to Hour and Month [29]

	Hour 0	Hour 1	Hour 2	Hour 3	Hour 4	Hour 5	Hour 6-22	Hour 23
January	100955.48	100910.65	100866.45	100856.45	100847.10	100836.45	...	100977.42
February	100993.45	100948.62	100904.48	100894.48	100885.17	100874.14	...	101011.38
March	100955.48	100910.65	100866.45	100856.45	100847.10	100836.45	...	100977.42
April	100974.67	100930.00	100886.00	100876.00	100866.67	100855.67	...	100992.33
May	100935.97	100892.90	100850.97	100841.94	100833.87	100825.16	...	100974.68
June-November	...	...	...	...	...	...		...
December	100955.48	100910.65	100866.45	100856.45	100847.10	100836.45	...	100977.42

4.3. LoRaWAN and Visualization

For the LoRaWAN server transmission, Figure 17 shows the server view of incoming FMS data, and Figure 18 displays the data visualization in Packetview. To transmit data via LoRaWAN to The Things Network server, the pressure and temperature data were encoded into two-byte payloads using the sflt162f encoding function from the LMIC Library. These payloads were split into upper and lower bytes for one-byte-at-a-time transmission. Once received by the server, the four-byte payload was decoded back into pressure and temperature data. Flood height calculations and more were performed on the server, and the organized data was sent to Packetview via Webhook integration.

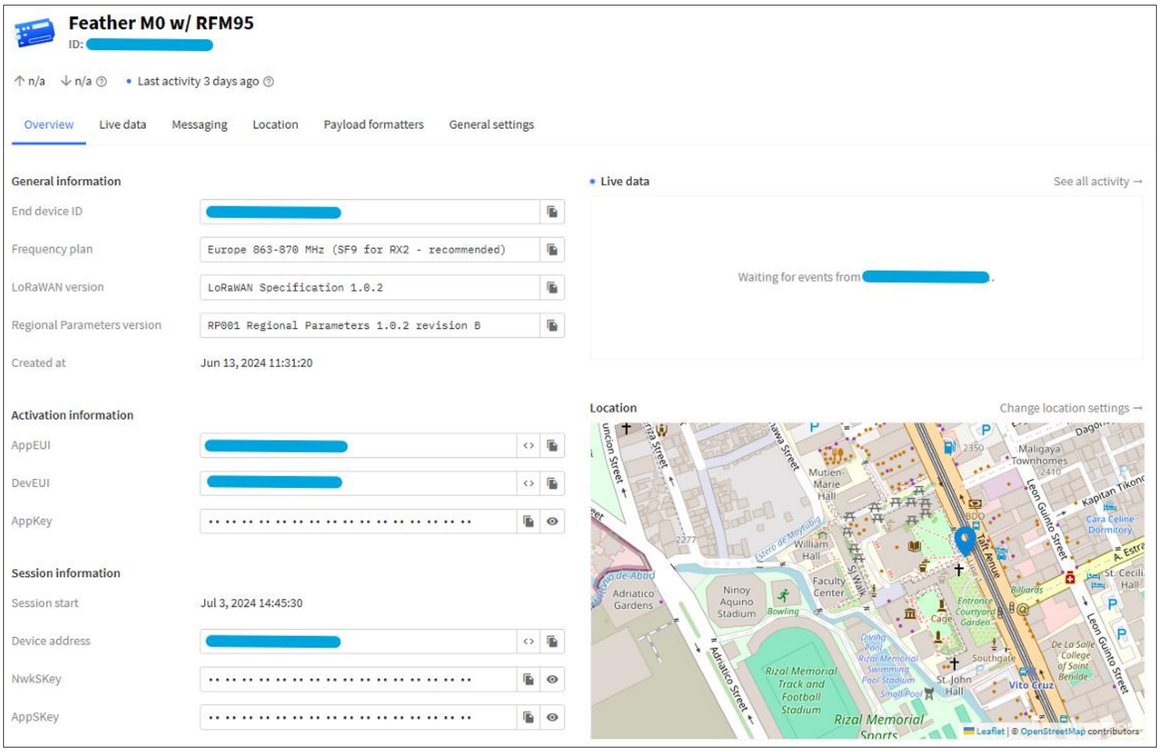

Figure 17. The Things Network Server

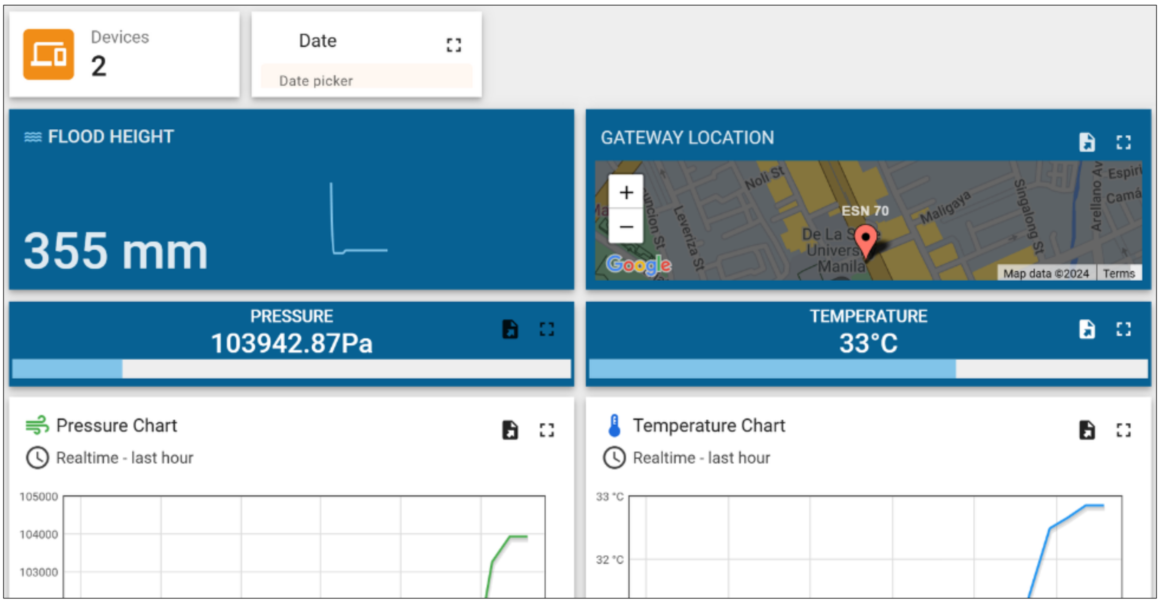

Figure 18. PacketView Flood Height Visualization

4.4. Power Consumption

To estimate the FMS's battery life, the total current consumption of the key components (Feather M0 microcontroller and DPS310 barometric pressure sensor) was calculated using their datasheet values, as shown in Table 2.

Table 2. Load Calculations of the FMS

Lora sleep current	300	uA	**Total sleep current**	300.5	uA
Sensor sleep current	0.5	uA	**Total active current**	120.0032	mA
Lora TX current	120	mA	**Sleep current / cycle**	299.9992	uA
Sensor active current	3.2	uA	**Active current / cycle**	0.2000	mA
Active time / cycle	1	s	**Chosen battery life**	1000	mAh
Cycle duration	600	s	**Calculated battery life**	1999.982	h

Given the sleep and active currents, and the cycle operation timing, the FMS's current draw per cycle was calculated. With a 1000mAh battery, the FMS's battery life is approximately 2000 hours or 83.3 days, expected due to the system's low power consumption. The solar panel must recharge the battery much quicker to be effective. Table 3 shows the solar panel load calculations.

Table 3. Load Calculations of the Solar Panel

Panel Watt	1	W	**Charger Efficiency**	50	%
Panel Voltage	6	V	**System Losses**	85.92	%
Battery Capacity	1000	mAh	**Solar Efficiency**	20	%
Battery Voltage	3.6	V	**Energy Need Fully Charge Battery**	1.782	Wh
Battery Depth of Discharge	50	%	**Solar Charging Rate**	0.08592	W
Lithium Charging Efficiency	99	%	**Hours to Fully Charge**	20.7402	h

Including efficiency and losses, the solar panel's fully charged time is 20.7 hours, or about a day. Given that the battery lasts 83 days, this solar panel should adequately supply the FMS for continuous operation.

To validate the calculations, the system battery was tested. The usable battery voltage in the system was from 4.18 V to 3.3 V. 4.18 V was obtained from fully charging the battery and measuring the voltage, while 3.3 V is the minimum allowable operating voltage of the microcontroller. Moreover, the battery voltage drops and gain from the system transmission and solar panel were also measured and calculated as shown in Table 4.

Table 4. Experimental Load Charge/Discharge Rates & Calculated System Life

Strong Sun	0.0467	V/hr	**Battery Full Charge with Strong Sun**	18.86	Hrs
Cloudy Sun	0.0222	V/hr	**Battery Full Charge with Cloudy Sun**	39.64	Hrs
Average Sun	0.0345	V/hr	**Battery Full Charge with Average Sun**	25.51	Hrs
Transmission	0.002679	V/hr	**Battery Life without Solar**	328.53	Hrs
			Battery Life with Solar (12 Hours Daylight, Cloudy Sun)	~Infinite Net V/hr: 0.0098	
			Battery Life with Solar (8 Hours Daylight, Cloudy Sun)	~Infinite Net V/hr: 0.0056	

With the usable battery voltage range and solar and system voltage gain and drop, the system life can be calculated as also shown in Table 4. The solar panel can charge the battery for 25.51 hours on average sun conditions, ranging from 39.64 to 18.86 hours. The calculated battery solar charge time is close to the calculated values, showing that the calculations were realistic. As for the battery life of the system without a solar panel, it would last only 328.53 hours. This is a big difference from the initial calculated 2000 hours. This may be due to the calculations not accounting for efficiency losses and battery discharge rates. Finally, when both charging and discharging are considered, it was calculated that the solar panel will be theoretically sufficient to operate the system indefinitely in 12 and 8-hour daylight scenarios. This demonstrated that the system could operate independently and self-sustaining even with less ideal weather conditions. However, the system requires further operational testing to be more certain.

4.5. Endurance

For the endurance testing, the test began at 5:00 PM and concluded at 9:30 PM the next day, lasting about 28 hours. Figure 19 shows a downward trend in measured pressure compared to atmospheric pressure, which was attributed to water evaporation. The water height measurements at various intervals were compared with the evaporation rate, and the plotted data showed an almost parallel trend to the calculated water level. This suggests minimal pressure drift over the 28-hour period. The FMS was able to accurately measure the atmospheric continuously throughout the endurance test with little to no pressure drift. This was significant as it ensured that the pressure readings are accurate, and thus produce accurate flood water height readings.

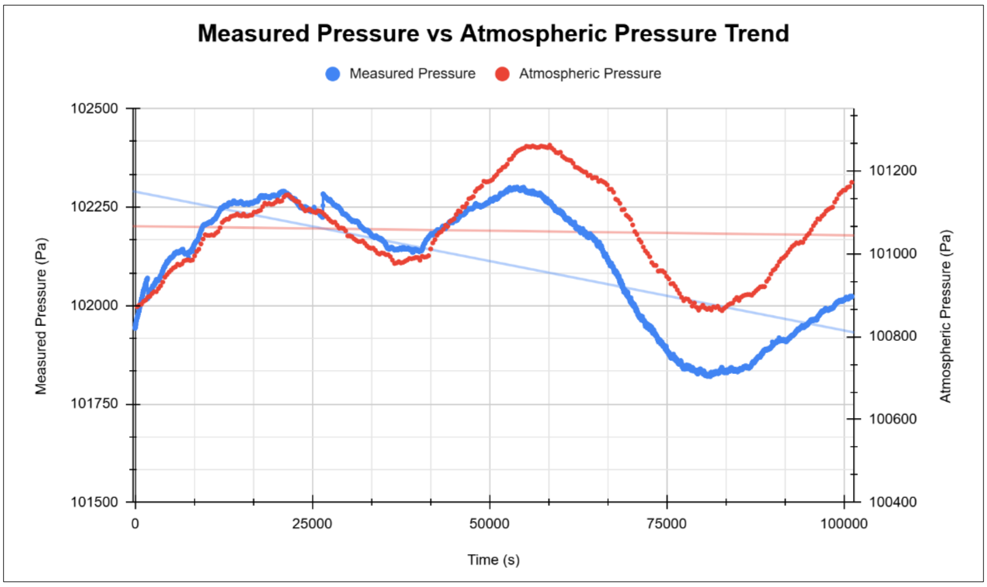

Figure 19. Endurance Test Measured Pressure vs Atmospheric Pressure Trend

4.6. Rain Simulation and Actual Rain Test

The results of the three simulated rain test trials are as follows: the first trial had a percentage error of 1.81% and a standard deviation of 6.92 mm. The second trial had a percentage error of 8.4% and a standard deviation of 15.55 mm. The third trial had a percentage error of 11.47% and a standard deviation of 44.15 mm. In the first trial, the accuracy was high, however this may have been a fluke compared to the second and third trials. The second trial had higher errors, possibly due to the stronger simulated rains finishing the trial earlier. Finally, the third trial showed the highest errors, near the FMS's allowable limit, likely due to transmission errors causing time lags in measured height. Despite higher errors, the FMS's performance was still acceptable, demonstrating its robustness.

The FMS was also tested in real rain, as shown in Figure 20. The water height recorded ranged from around 20 mm to 85 mm, with a brief movement of the system at the 1100-second mark. The average percentage error was 2.65% with a standard deviation of 1.708 mm. This was a contrast compared to the simulated rains with higher percentage errors. This result supports the findings from the disturbance and accuracy tests, showing that the error remains low in real rain scenarios.

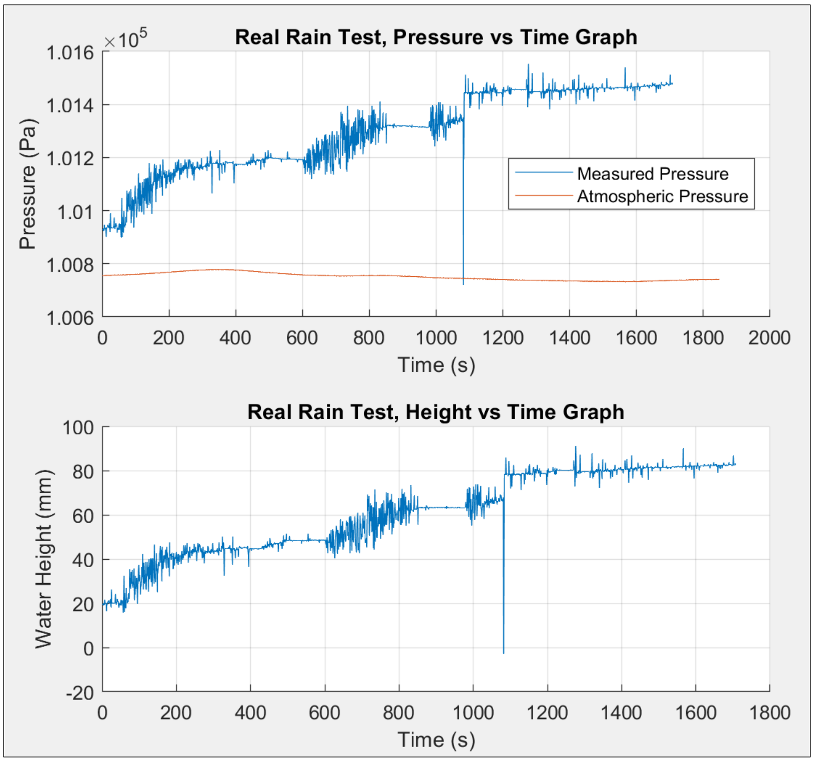

Figure 20. Real Rain Test, Pressure vs Time & Water Height vs Time Graph

5. Conclusion

The development of a smart IoT urban flood monitoring system using a high-performance pressure sensor with LoRaWAN shows promise for implementation in flood-prone urban areas that can greatly benefit from the dissemination of important flood information. Such FMS' could play an integral role in increasing the safety and security of various flood-prone areas within the Philippines and allowing for better government aid and flood responses. This can be shown as the hardware components, including the pressure sensor mount, PVC connections, and electronic enclosure, were validated through ANSYS simulations. LoRaWAN communication was integrated to transmit pressure and temperature data to a remote server while the collected data is visualized on the Packetview platform. The testing showed the FMS had high accuracy, with errors as low as 1.12%. The FMS was resistant to disturbances as it can stabilize within 0.5s with an acceptable error range.

For continued improvement in the development of this novel LoRaWAN-based barometric FMS, it is recommended to conduct further testing of the FMS with multiple elbow configurations (i.e., increasing the number of elbow bends). This would provide flexibility of the device when the installation areas are not optimal. Improving the fastening mechanisms is also recommended for the deployment and to simulate the system's durability against effects of wind forces or vibrations caused by flooding. This is to ensure that the FMS will be able to operate under harsher weather conditions. Lastly, optimizing the placement is also recommended based on gateways by determining suitable locations for effective radio communication and deploying multiple devices to test the performance at different environmental conditions, which verify its sustained functionality.

6. Declarations

6.1. Author Contributions

Conceptualization, A.Y.C.; methodology, M.C.L.T., J.A.T.B., S.M.E.V.D., A.V.M.L., and M.G.M.P.; software, M.C.L.T., J.A.T.B., S.M.E.V.D., A.V.M.L., and M.G.M.P.; validation, M.C.L.T., J.A.T.B., S.M.E.V.D., A.V.M.L., and M.G.M.P.; formal analysis, M.C.L.T., J.A.T.B., S.M.E.V.D., A.V.M.L., and M.G.M.P.; investigation, M.C.L.T., J.A.T.B., S.M.E.V.D., A.V.M.L., and M.G.M.P.; resources, M.C.L.T., J.A.T.B., S.M.E.V.D., A.V.M.L., M.G.M.P., and A.Y.C.; data curation, M.C.L.T., J.A.T.B., S.M.E.V.D., A.V.M.L., and M.G.M.P.; writing—original draft preparation, M.C.L.T., J.A.T.B., S.M.E.V.D., A.V.M.L., and M.G.M.P.; writing—review and editing, M.C.L.T., J.A.T.B., S.M.E.V.D., A.V.M.L., M.G.M.P., and A.Y.C.; visualization, M.C.L.T., J.A.T.B., S.M.E.V.D., A.V.M.L., and M.G.M.P.; supervision, A.Y.C.; project administration, M.C.L.T. and A.Y.C.; funding acquisition, A.Y.C. All authors have read and agreed to the published version of the manuscript.

6.2. Data Availability Statement

The data presented in this study are available on request from the corresponding author.

6.3. Funding and Acknowledgements

The authors express their gratitude for the technical assistance and materials provided by the Mechanical Engineering Department, Packetworx, and Infineon Philippines. Also, the authors would also like to thank and acknowledge the Research and Grants Management Office of De La Salle University for their funding in the research.

6.4. Institutional Review Board Statement

Not applicable.

6.5. Informed Consent Statement

Not applicable.

6.6. Declaration of Competing Interest

The authors declare that they have no known competing financial interests or personal relationships that could have appeared to influence the work reported in this paper.

7. References

[1] World Bank Group (2024). Philippines - Vulnerability. Climate Change Knowledge Portal. The World Bank Group, Washington, D.C., United States. Available online: https://climateknowledgeportal.worldbank.org/country/philippines/vulnerability (accessed on November 2024).

[2] NOAH. (2024). Nationwide Operational Assessment of Hazards. Project NOAH, Quezon City, Philippines. Available online: https://noah.up.edu.ph/ (accessed on November 2024).

[3] Lagmay, A. M., Mendoza, J., Cipriano, F., Delmendo, P. A., Lacsamana, M. N., Moises, M. A., ... & Tingin, N. E. (2017). Street floods in Metro Manila and possible solutions. Journal of Environmental Sciences, 59, 39-47. doi:10.1016/j.jes.2017.03.004.

[4] Hassan, W. H., Jidin, A. Z., Aziz, S. A. C., & Rahim, N. (2019). Flood disaster indicator of water level monitoring system. International Journal of Electrical and Computer Engineering, 9(3), 1694–1699. doi:10.11591/ijece.v9i3.pp1694-1699.

[5] Rani, D. S., Jayalakshmi, G. N., & Baligar, V. P. (2020). Low Cost IoT based Flood Monitoring System Using Machine Learning and Neural Networks: Flood Alerting and Rainfall Prediction. 2nd International Conference on Innovative Mechanisms for Industry Applications, ICIMIA 2020 - Conference Proceedings, 261–267. doi:10.1109/ICIMIA48430.2020.9074928.

[6] Retamar, A. E., Guba, G., Lopez, G. V., Paler, H. B., Javier, J., Garcia, F. C. C., Badong-Carlos, J., Capito, J., Mosquera, I. C., De Paz, M., & Yabut, J. J. (2017). HydroMet: Deployment of a large-scale nationwide hydrometeorological sensor network for flood warning and monitoring. GHTC 2017 - IEEE Global Humanitarian Technology Conference, Proceedings, 2017-January, 1–10. doi:10.1109/GHTC.2017.8239323.

[7] Dswilan, S., Harmadi, & Marzuki. (2021). Flood monitoring system using ultrasonic sensor SN-SR04T and SIM 900A. Journal of Physics: Conference Series, 1876(1), 12003. doi:10.1088/1742-6596/1876/1/012003.

[8] Natividad, J. G., & Mendez, J. M. (2018). Flood Monitoring and Early Warning System Using Ultrasonic Sensor. IOP Conference Series: Materials Science and Engineering, 325(1), 12020. doi:10.1088/1757-899X/325/1/012020.

[9] Binti Zahir, S., Ehkan, P., Sabapathy, T., Jusoh, M., Nasrun Osman, M., Najib Yasin, M., Abdul Wahab, Y., Hambali, N. A. M., Ali, N., Bakhit, A. S., Husin, F., Kamil, M. K. M., & Jamaludin, R. (2019). Smart IoT Flood Monitoring System. Journal of Physics: Conference Series, 1339(1), 12043. doi:10.1088/1742-6596/1339/1/012043.

[10] Yuliandoko, H., Subono, Wardhany, V. A., Pramono, S. H., & Siwindarto, P. (2018). Design of flood warning system based IoT and water characteristics. Telkomnika (Telecommunication Computing Electronics and Control), 16(5), 2101–2110. doi:10.12928/TELKOMNIKA.v16i5.7636.

[11] Yoeseph, N. M., Purnomo, F. A., Hartono, R., & Nuryani. (2022). Lora-based IoT sensor node for Real-time Flood Early Warning System. IOP Conference Series: Earth and Environmental Science, 986(1), 12060. doi:10.1088/1755-1315/986/1/012060.

[12] Zakaria, M. I., Jabbar, W. A., & Sulaiman, N. (2023). Development of a smart sensing unit for LoRaWAN-based IoT flood monitoring and warning system in catchment areas. Internet of Things and Cyber-Physical Systems, 3, 249–261. doi:10.1016/j.iotcps.2023.04.005.

[13] Rahayu, F., Zuchriadi, A., Fauzi, A. F., & Dewantara, A. B. (2022). Prototype Flood Detection Water Level Monitoring IoT Web Based With Ultrasonic Sensor HC-SR04. Jurnal Mantik, 6(36), 2006–2014.

[14] Ming Ray, K., & Mustafa, F. (2023). Solar Powered IoT Flood Detector. Progress in Engineering Application and Technology, 4(2), 332–344.

[15] Tolentino, L. K. S., Baron, R. E., Blacer, C. A. C., Aliswag, J. M. D., De Guzman, D. C. E., Fronda, J. B. A., Valeriano, R. C., Quijano, J. F. C., Padilla, M. V. C., Madrigal, G. A. M., Valenzuela, I., & Fernandez, E. (2023). Real Time Flood Detection, Alarm and Monitoring System Using Image Processing and Multiple Linear Regression. SSRN Electronic Journal, 7(1), 1-21. doi:10.2139/ssrn.4319789.

[16] Lo, S. W., Wu, J. H., Lin, F. P., & Hsu, C. H. (2015). Visual sensing for urban flood monitoring. Sensors (Switzerland), 15(8), 20006. doi:10.3390/s150820006.

[17] Hashemi-Beni, L., Puthenparampil, M., & Jamali, A. (2024). A low-cost IoT-based deep learning method of water gauge measurement for flood monitoring. Geomatics, Natural Hazards and Risk, 15(1), 2364777. doi:10.1080/19475705.2024.2364777.

[18] Bande, S., & Shete, V. V. (2018). Smart flood disaster prediction system using IoT & neural networks. Proceedings of the 2017 International Conference on Smart Technology for Smart Nation, SmartTechCon 2017, 189–194. doi:10.1109/SmartTechCon.2017.8358367.

[19] Sandhya, T., Shalini, M., Kumar, C., Vaishnavi, Priyanka, Rao, D. S. N. M., & Singh, D. (2023). Lora Technology for Flood Monitoring and Warn System. E3S Web of Conferences, 430. doi:10.1051/e3sconf/202343001168.

[20] Saparudin, F. A., Halim, M. S., Amani Ibrahim, N. S., & Baharom, M. F. (2024). Real-Time Flood Monitoring Using Mobile LoRaWAN IoT Gateway: A Case Study of the Muar River Catchment. ICoCET 2024 - 2024 IEEE 1st International Conference on Communication Engineering and Emerging Technologies, 1–4. doi:10.1109/ICoCET63343.2024.10730107.

[21] Gunanandhini, S., Livyashree, M., Maheshwaran, R. R., Palanisamy, K. S., & Niranjan Kumar, V. (2024). Forecasting and Real Time Flood Monitoring System using IoT. 10th International Conference on Advanced Computing and Communication Systems, ICACCS 2024, 1228–1233. doi:10.1109/ICACCS60874.2024.10716883.

[22] Garcia, F. C. C., Retamar, A. E., & Javier, J. C. (2016). A real time urban flood monitoring system for metro Manila. IEEE Region 10 Annual International Conference, Proceedings/TENCON, 2016-January, 1–5. doi:10.1109/TENCON.2015.7372990.

[23] Azid, S., Sharma, B., Raghuwaiya, K., Chand, A., Prasad, S., & Jacquier, A. (2015). SMS based flood monitoring and early warning system. ARPN Journal of Engineering and Applied Sciences, 10(15), 6387–6391.

[24] Dublin, A. C., Arce, M., Ortiz, E., Wong, L. M., Villaruel, K. P., Arante, H. R., Co, D., Chua, A., Sybingco, E., & Roque, M. A. (2024). A Novel Cost-Effective Pressure Sensor Based Flood Monitoring System with IoT. ASEAN Engineering Journal, 14(3), 53–61. doi:10.11113/aej.V14.20668.

[25] Arce, M., Ortiz, E., Villaruel, K., & Wong, L. Development of an Urban Flood Monitoring System with Visualization using IoT Connectivity. Undergraduate Thesis, De La Salle University Manila, Manila, Philippines.

[26] Lee, Y. J., Hwang, J. Y., Park, J., Jung, H. G., & Suhr, J. K. (2024). Deep Neural Network-Based Flood Monitoring System Fusing RGB and LWIR Cameras for Embedded IoT Edge Devices. Remote Sensing, 16(13), 2358. doi:10.3390/rs16132358.

[27] William, P., Oyebode, O. J., Ramu, G., Lakhanpal, S., Gupta, K. K., & Al-Jawahry, H. M. (2023). Framework for IOT Based Real-Time Monitoring System of Rainfall Water Level for Flood Prediction Using LSTM Network. Proceedings - 2023 3rd International Conference on Pervasive Computing and Social Networking, ICPCSN 2023, 1321–1326. doi:10.1109/ICPCSN58827.2023.00222.

[28] Prakash, C., Barthwal, A., & Acharya, D. (2023). An IoT-based system for monitoring and forecasting flash floods in real-time. Journal of Earth System Science, 132(4), 159. doi:10.1007/s12040-023-02172-4.

[29] Meteostat (2024). Air Pressure: Manila, Philippines. Meteostat. Available online: https://meteostat.net/en/station/98425 (accessed on November 2024).